Tribology International 104 (2016) 272–284

Contents lists available at ScienceDirect

Tribology International

journal homepage: www.elsevier.com/locate/triboint

Characterisation of flame-generated soot and soot-in-oil using electron tomography volume reconstructions and comparison with traditional 2D-TEM measurements

O. Orhan [a], E. Haffner-Staton [a], A. La Rocca [a,*], M. Fay [b]

[a] Department of Mechanical Materials and Manufacturing Engineering, University Park, Nottingham, NG7 2RD UK
[b] Nottingham Nanotechnology and Nanoscience Centre, University Park, Nottingham, NG7 2RD UK

ARTICLE INFO

Article history:
Received 30 June 2016
Received in revised form
7 September 2016
Accepted 8 September 2016
Available online 9 September 2016

Keywords:
Soot characterisation
2D-TEM
Fractal dimension
Electron tomography
Volume reconstructions

ABSTRACT

This work characterises soot nanoparticles by electron tomography using Weighted Back Projection algorithm and appraises the uncertainties in two-dimensional calculations by comparison with 3D parameters for flame-generated soot and diesel soot-in-oil. Bright field TEM was used to capture 2D images of soot. Large uncertainties exist in 2D-measured morphological parameters. The flame-generated particle showed an extensive 3D structure while the soot-in-oil was notably two-dimensional. Morphological parameters of flame-generated soot and diesel soot-in-oil were different; primary particles, volume, and surface area varied significantly over the range of viewing angle, with differences as large as 60%. 2D flame-generated soot volume underestimated 3D measurements by 38%; soot-in-oil 2D- and 3D-derived volumes were within 4%. 2D calculations of fractal dimension generally underestimate the 3D value.

1. Introduction

The lubricant for the automotive market of 2030 must offer protection to smaller engines with tighter tolerances. New motor oil formulations will need to reduce the frequency of repairs, prolong engine life, and improve fuel efficiency and allow for longer intervals between oil changes. It is well established that oil thickening has a complex dependence on soot albeit challenges associated with poor characterisation of suspensions, stability of dispersion and increase in viscosity remain unresolved. Studies of soot in automotive lubricants have mainly focused on its percentage by weight as the primary correlative factor affecting oil properties, such as viscosity and engine wear. Due to the fractal and highly irregular nature of soot particles more quantitative characterisation techniques would assist in lubricant formulation.

Soot is formed during combustion of hydrocarbon fuel in automotive engines due to non-stoichiometric, incomplete combustion conditions. Fuel-rich zones form due to inadequate mixing of the fuel-air mixture prior to ignition, and lead to the formation of soot [1]. Low temperature conditions in the engine, such as during start-up, also causes insufficient vaporisation of fuel leading the presence of liquid fuel droplets, and fuel films forming on the walls of the cylinder and on top of the piston [1]. Soot can form directly from pyrolysis of liquid fuel droplets [2,3], and the pool-fires that results from the fuel films have been identified as perhaps the most important source of soot in gasoline engines [1,2,4,5].

Three main stages are generally agreed upon as those that lead to the formation of soot: nucleation, growth, and oxidation [1,6]. Radical polymerisation reactions involving acetylene and other small, unsaturated molecules leads first to the formation of small aromatic systems such as benzene, under high temperature conditions (1000–2800 K) [1,7]. Alongside radical recombination of growing aromatics, the polymerisation reactions result eventually in large polyaromatic hydrocarbons (PAH's) of around 500–1000 amu [7]. Coagulation of these extended aromatic systems, concurrent with a surface growth mechanism involving gas phase species leads to the formation of so-called primary particles, with diameters typically 20–50 nm. Primary particles are spherical and possess an inner-core and outer-layer structure [8]. The inner core, roughly 10 nm in diameter, comprises several fullernoid spherules 4–5 nm in diameter centred on a 1 nm nucleus, surrounded themselves by a distorted, bending carbon structure [8,9]. The outer layer is of similar thickness, formed from a concentric, onion-like arrangement of graphitic microcrystallites roughly 1 nm thick and 3.5 nm wide [9]. The primary particles coagulate to create chain and cluster-like soot agglomerates usually 50–500 nm in size, displaying fractal geometries. Oxidation is pervasive throughout soot formation, and species such as O_2, OH, O, CO_2, and H_2O act to reduce soot concentration at each stage [7].

* Correspondence to: Engine Research Group, Department of Mechanical, Materials and Manufacturing Engineering, University Park, The University of Nottingham, NG7 2RD, UK.
E-mail address: antonino.larocca@nottingham.ac.uk (A. La Rocca).

http://dx.doi.org/10.1016/j.triboint.2016.09.015

The major fraction of soot produced in the cylinders is removed with the exhaust gases; a small amount of the soot transfers to the lubricant oil film lining the walls of the cylinder via a thermophoretic mechanism, where it is scraped into the sump. Blow-by gases passing the piston rings also lead to entrainment of soot within the oil [10].

High-resolution imaging and characterisation of soot permits effective study of soot formation, soot as an atmospheric pollutant, soot-related engine wear, and detailed design of improved lubricant oils, fuel additives, and particulate filters.

As soot particles are on the scale of nanometres, electron microscopy, and particularly transmission electron microscopy (TEM), is the preferred method of capturing images of particles. Characterisation of morphological values can also be achieved via alternative means, such as nanoparticle tracking analysis (NTA), and dynamic light scattering (DLS). These methods track motion of particles and use particle motion as a means to calculate hydrodynamic size of particles, as well as size distributions and number concentrations [11].

TEM has been used extensively in the characterisation of both exhaust soot and so-called soot-in-oil (soot entrained within the lubricant oil) from a variety of automotive engine and fuel sources [1,6,12–16]. A number of studies have also chosen to characterise carbon black alongside or in place of engine soot [6,13,17–21]. Carbon black (CB) refers to a carbonaceous material commercially produced by incomplete combustion in hydrocarbon flames. With relation to soot, study of carbon black has focused on comparison of their morphology because of the similarity between them, but has also seen CB used as a convenient surrogate for genuine engine soot. Production of engine soot for study (either exhaust or soot-in-oil) generally requires many hours (often in excess of 30) of running test engines [1,12], a process much more costly in terms of both time and resources than those used to produce carbon black. As such, CB has been used to study oxidation of soot [13,18], atmospheric chemistry [17], and wear and viscosity effects in lubricant oils [6,19–21].

Due to the complex, fractal nature of soot there is no definitive parameter that will satisfactorily characterise the 3D nature of a soot particle, and as such a range of measurements are often taken. Those generally used to characterise soot are maximum projected length and width (or alternatively skeletal length and width), radius of gyration, number of primary particles, surface area, volume, and fractal dimension [1,12,22–25].

As TEM images are 2D projections of 3D objects, calculations of some 3D parameters are inferred by application of approximations. For example, when calculating the number of constituent primary particles, the primary particles are considered spherical and identical in size, and experimentally determined correction factors are used to account for particle overlap [22–24]. Volume of agglomerates has been calculated simply by multiplying the values for individual particles by the number of primary particles, discounting any overlap of particles that could occur [25]. Alternatively, volume and surface area have been estimated by establishing a sphere to represent the particle with diameter the mean of the maximum and minimum dimensions of the particle as seen in the TEM images [26]. In such cases, differences of up to 2 orders of magnitude can be found compared with 3D reconstructed volumes [27]. Whilst free of use of empirical correction factors, fractal dimension and radius of gyration are measured based on 2D images. As the viewing angle is altered, regions of the particle not directly joined in space can appear to be so, and pores can appear or be hidden, causing misleading results [27]. Indeed, the orientation of soot particles on the TEM grid is a largely ignored source of uncertainty. As viewing angle of a particle is varied, it is obvious that the apparent morphology and therefore projection area will change, particularly so when considering the fractal nature of soot particles. Projected area is used when determining number of primary particles, volume, surface area, radius of gyration, and fractal dimension [22–25], and raises the question of which viewing angle should be used in 2D measurements. Of course, all randomly orientated views are equally valid in this respect, but may result in significantly different values if the projection-area of the particle is significantly different. This issue is potentially more significant if there is any non-random orientation introduced by deposition of the soot onto the TEM support film.

For the reasons just discussed, and despite its wide use, the 2D limitations of TEM means the true 3D nature of soot particles cannot be accounted for entirely. Rogak et al. [28] suggested that 2D measurements would be underestimated in the range of 10–20%, and works by La Rocca and by van Poppel found differences of up to two orders of magnitude when considering hydrodynamic volume and surface area [16,27]. Patel and Aswath [29] have used traditional TEM to examine soot extracted from crankcase and cylinder wall of a Mack T-12 engine used to study the wear tracks and tribofilms generated on the groove piston rings. Hu et al. have described the influence of soot contamination on the behaviour of engine oils and discussed the mechanisms of wear induced by soot particles and their interaction with oil additives [30]. Absorption and agglomeration effects were the principal factors affecting the tribological mechanism. The surface area of agglomerates plays an important role as particles can absorb molecules of oil and react with one another to form larger agglomerates. Lahouij et al. observed that as soot concentration builds within the oil phase lubricant performance is adversely affected, particularly in lower quality products, as viscosity increases impede oil flow [31]. They also considered the behaviour of the soot aggregates when shear forces are applied to agglomerates to understand the process of deformation of soot particles. Agglomerates and single particles resulted to be resistant to load. Wear can occur where the oil film is thinner than the size of soot particles as soot is hard enough to abrade some metal engine parts [31]. Agglomeration of soot can cause oil starvation leading to metal-metal contact and consequent wear, as well as reducing the effectiveness of anti-wear agents. The fractal dimension of exhaust soot particle is affected by the combustion of anti-wear additives; a decrease in fractal dimension of the aggregate particles was measured when fuel was blended with the additive [32]. Chemical and morphological differences observed between gasoline and diesel soot lead to changes in the polarity and hardness of the soot particles and affect the wear mechanism in the engines [33]. As reported by Cui et al. [34] agglomerate morphology and soot surface available for coverage also play an important role in design and architectural features of new viscosity modifiers and dispersants to prevent soot aggregation. As engine wear and changes in lubricant oil viscosity due to soot are known to depend on the surface area and volume of the particles [16,35], and the environmental and health damaging effects upon the particles size [16,36], surface area [35], and fractal dimension [35,37], accurate explanation and predictions of such effects in turn requires accurate characterisation of the particles involved.

Tomographic reconstructions of soot from used engine oil samples using TEM and the methodology described in this work helps to better extract parameters necessary to potentially understand the role of soot particles in the tribological behaviour of engine lubricating oils. This work demonstrates the feasibility of electron tomography for three-dimensional characterisation of soot-in-oil nanoparticles; proposing a new methodology to give measurable 3D soot models that are of practical use to industry. It also highlights that 2D electron microscopy is associated with significant uncertainties when it comes to calculation of 3D morphological properties.

2. Electron tomography of soot nanoparticles

Electron tomography (ET) can be used to reconstruct a 3D volume of a particle from a series of aligned 2D TEM images. Tilting the specimen holder in the TEM machine and capturing images at incremental angles allows us to record a so-called 'tilt-series' of images. Due to mechanical limitations, a tilt-series is usually captured over a ± 60–70° range. Small shifts can occur between each increment meaning images have to undergo an alignment process, often achieved through cross-correlation and tracking through the tilt-series of high contrast markers (usually gold nanoparticles) that have been added to the specimen [38].

High quality markerless alignment methods exist for high-contrast species using recognisable areas of the image to align the series, but may be inadequate for soot because of the extremely low contrast [16,38].

The reconstruction of the 3D structure from the tilt-series is based upon the central section theorem, which states that the complete set of Fourier transforms of the 2D projections are contained within the Fourier transform (FT) of the 3D specimen, and therefore an inverse FT links the tilt-series to the true 3D structure [38]. In practice, the inverse FT is unfeasible due to difficulties with interpolation in Fourier space [38] and methods based upon back projection are often employed. Two commonly used back projection methods are weighted back projection (WBP), and the simultaneous iterative reconstruction technique (SIRT) [38], and both have been used in the study of soot [16,27,37]. WBP is based on a real-space application of the Fourier theory just mentioned, assuming that projections represent the amount of mass the rays travelled through. Its broad application is based on its computational simplicity [38]. SIRT involves the computation of projections from an estimated tomogram, and uses the error between actual and computed projections to refine the reconstruction.

Another more recent approach is the discrete algebraic reconstruction technique (DART), which has been applied to the quantitative study of several types of nanoparticles, including carbon nanotube structures [39,40]. DART models the reconstruction problem as a large system of linear equations that are solved by iterative methods, and can lead to improved reconstructions at the expense of increased computational cost [40]. Iterative techniques are known to show improved contrast compared to WBP, but are considerably more computationally expensive [41].

As a tilt-series cannot usually be captured over the entire 360° range, there is essentially a missing 'wedge' of information in Fourier space that leads to artefacts and elongation distortions in the reconstruction. To combat this, a dual-axis tilt-series may be formed by performing a second tilt perpendicular to the first, reducing the missing information to a smaller pyramidal shape, and improving the reconstruction [38,42]. Alternate tilt-series exist to improve reconstruction depending on the mechanical limitations of the equipment, including 360° tilting and conical tilts [42].

Noise can have a profoundly destructive effect on the reconstruction process, and thus efforts must be made to reduce noise. Methods of noise reduction are often categorised as: linear, non-linear, and anisotropic [43]. Linear methods average voxels based on the neighbourhood value, and disregard any structural intricacies. Non-linear methods allow the consideration of structures (particularly those within particles) by applying stronger filtering in more homogeneous areas of contrast, and reduced smoothing in areas of large contrast gradients. Anisotropic methods allow adjustment of the strength and direction of filtering to maximise results. An in-depth discussion on the issues of noise in tomograms is provided in [43].

For quantitative means, a segmentation process must be employed to establish the boundary between the particle voxels and those of the background. As both the particle and grid are primarily carbon, contrast is low meaning automated segmentation methods based on thresholding are often inaccurate. Manual segmentation has often been preferred in these types of studies because of this, but is a lengthy and labour intensive process requiring skilled operators [16,44]. Another issue with manual segmentation is subjectivity. The boundary between background and particle is often unclear, particularly so because of the transparent nature of particles in TEM images, and leads to uncertainty in interpreting the information at the edge of the particle [16]. As the segmentation directly determines the outline of the particle, it must also directly affect the values of the morphological parameters that will be calculated, and as such accuracy in segmentation is of upmost importance.

Despite extensive use in the study of biological systems and nanoparticles [38], these studies represent the only forays of ET into the field of soot study. The creation of accurate 3D models of soot particles would allow the discussed morphological parameters to be calculated without the need for approximations or experimentally determined correction factors, and removes the uncertainties associated with lack of depth in the 2D images [37].

Unfortunately, the well-established ET techniques widely used in the study of biological systems and metal nanoparticles are not easily extended to the study of soot. The light element nature of soot means TEM images are extremely low contrast, and combined with their small size leads to difficulties in reconstruction, such as alignment and segmentation [16].

In addition to being a fundamental requirement for the reconstruction of 3D volumes, the tilt-series created also provided an ideal set of data with which to outline the uncertainties in 2D measurements associated with viewing angle. In this study the extent to which particle orientation (effectively the viewing angle) can cause uncertainty in measurements commonly used to characterise soot particles is presented and quantified. The work outlines the need for advancement in ET methods for such species. The findings are presented for particles of flame-generated carbon black, and soot-in-oil from a diesel engine. Flame-generated soot provided a useful preliminary species for study, as the lack of oil contamination meant that application of ET methods was simpler. Following the successful ET reconstruction of this species, the more problematic of soot-in-oil reconstruction was tackled. Carbon black provides an interesting comparison to soot-in-oil because of the role it has enjoyed as a surrogate for soot in various studies [6,13,17–21]. By considering these two very different sources of soot, we can also evaluate the role that the source of the soot plays in the accuracy of 2D calculations.

3. Experimental setup and sample preparation

Two model systems of soot were used in this investigation: flame-generated soot and diesel engine soot extracted from oil in the sump [12]. Flame generated soot was deposited directly onto the TEM grid. Mineral oil is a known and severe contaminant under the electron beam; so to prime the soot-in-oil for study, an extraction process using heptane was employed according to that used in previous work [1]. The samples of soot extracted from engine oil were prepared by diluting the oil at a dilution ratio of 1:60 in heptane. The heptane solution is at a suitably low viscosity to allow deposition onto TEM grids. Following deposition, the solvent evaporates rapidly to leave soot particles of varying sizes, without aggregation during drying on the grid. This process puts little strain on the soot aggregates and reveals a structure typical of the soot as it was in the engine oil. Samples were then subjected to close-to-vacuum conditions at ambient temperature in order to enhance the evaporation of the solvent. At this stage, the level of

contamination remains too high to obtain repeatable imaging for tilt series but allows standard TEM of the soot structure. Two further stages of diethyl bathing were employed to reduce contamination. This proposed cleaning procedure is capable of producing a soot sample extracted from oil suitable for a high-angle tilt-series acquisition. Gold fiducial markers for image alignment were added to the grid post-preparation suspended in heptane, the solvent evaporating and leaving the particles dispersed on the grid. The gold nanoparticles obtained from MP Biomedicals were spherical with diameters of 10 nm (± 3 nm). Soot characterisation was carried out at the Nottingham Nanotechnology and Nanoscience Centre using a JEOL 2100F TEM equipped with a Gatan Orius CCD camera operating at 100 kV.

4. Calculation of parameters

Flame-generated soot and soot-in-oil particles were characterised in terms of projection area, number of primary particles, surface area, volume, radius of gyration, and fractal dimension using TEM images from the tilt-series that were collected for the reconstructions. Traditional TEM images, untilted, for flame generated soot and soot in oil, are provided in Fig. 1.

Flame-generated soot was characterised every 4° through the complete $\pm 60°$ range of the tilt-series used; a total of 31 out of the 121 images. Due to corruption of some of the images in the tilt-series, soot-in-oil particles were characterised every 4° from $-60°$ to $+51°$ across the tilt-series, a total of 29 of the 112 images.

4.1. Projection-area derived measurements

The projection area, A_{eff}, of particles in TEM images was calculated through region of interest selection using open architecture imaging software ImageJ. Similar methods were employed for evaluating the mean diameter of the spherical primary particles, by measuring only those clearly visible in the TEM images.

Medalia et al. outlined the initial method for the calculation of the number of constituent primary particles in their studies of carbon black in the late 1960's. They proposed the following power-law relationship between the projection area of agglomerates and the number of constituent primary particles [45–47]:

$$N_p = \left(\frac{A_{eff}}{A_p}\right)^{\alpha} \quad (1)$$

where N_p is the number of primary particles in the agglomerate, A_p is the cross-sectional area assumed representative of all primary particles, and α is a constant accounting for overlap of primary particles, empirically determined as 1.09. Primary particles are assumed spherical, with volume and area via:

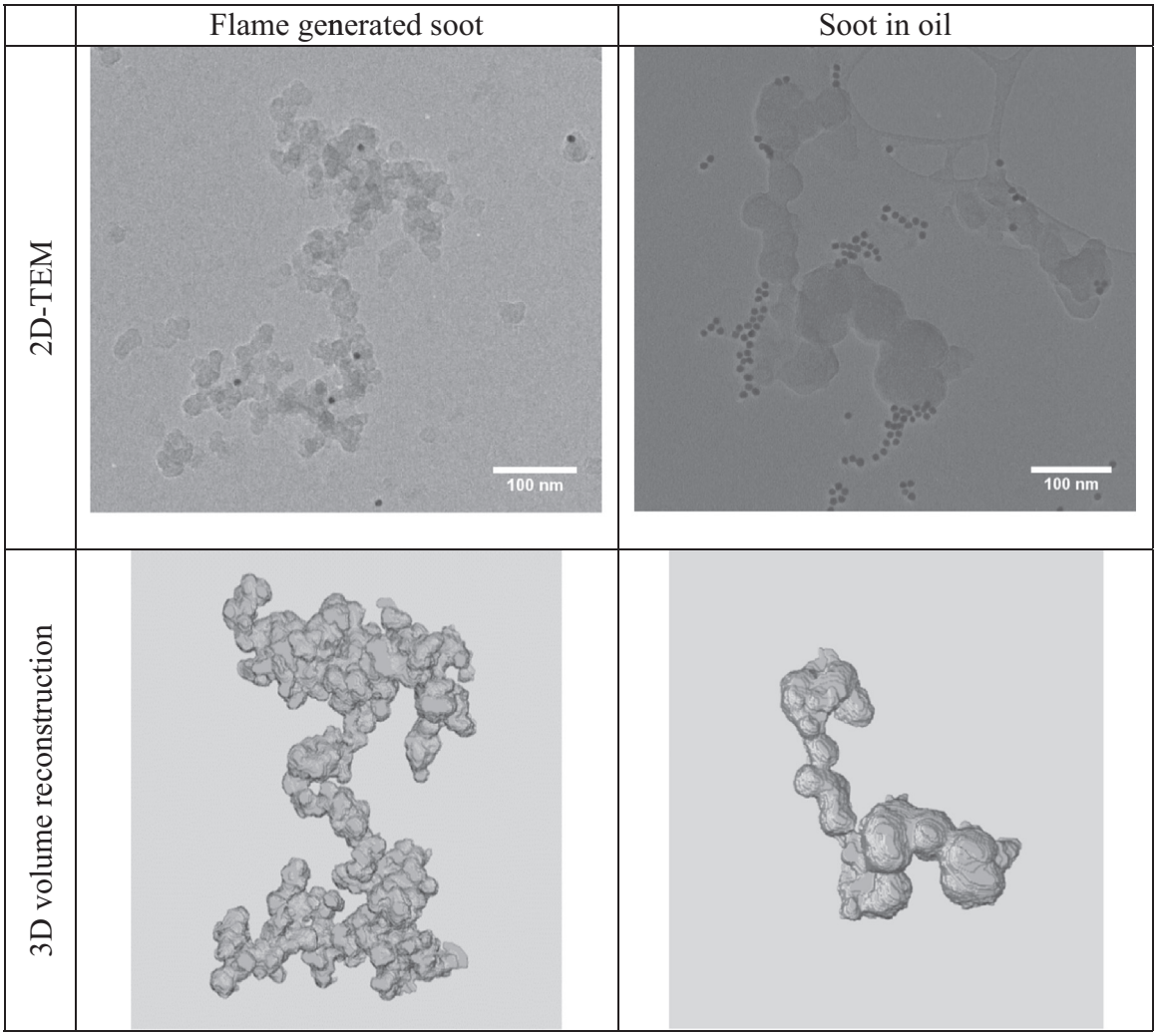

Fig. 1. Traditional 2D-TEM (untilted) and 3D volume reconstruction of flame generated soot and soot-in-oil.

$$V_p = \frac{4A_p^{3/2}}{3\sqrt{\pi}} \tag{2}$$

$$A_p = \frac{\pi d_p^2}{4} \tag{3}$$

Köylü et al., in their study of soot agglomerates, proposed a slight alteration to this equation based on their study of simulated aggregates [22]:

$$N_p = k_a\left(\frac{A_{eff}}{A_p}\right)^{\alpha} \tag{4}$$

Their empirical methods determined k_a and α as 1.16, and 1.10 respectively, together approximately accounting for overlap of primary particles. More recently, Neer and Köylü refined these values to $k_a = 1.15$, and $\alpha = 1.09$ [23], and it is this version of the equation that was used to estimate the number of primary particles per agglomerate in this work.

Total surface area and volume of agglomerates was calculated simply via multiplication of primary particle surface area and volume by number of constituent primary particles:

$$V = \frac{\pi d_p^3}{6} N_p \tag{5}$$

$$A_s \approx N_p \pi d_p^2 \tag{6}$$

4.2. Fractal dimension

In 1975 Mandelbrot proposed the concept of fractals to describe a family of irregular and fragmented shapes not easily accountable with Euclidean geometry [48]. A determinant fractal is a shape that displays true self-similarity, appearing identical at all scales of resolution. Soot particles are not truly self-similar but do possess a degree of self-similarity on average, and may be considered 'mass fractals' [28]. Mass fractals obey a power-law relationship between density (or mass, M) and distance from the centre of mass of the object (R), $M \sim R^{D_f}$ [22,23,49].

Alternatively, this may be expressed in terms of number of constituent primary particles (N), radius of gyration (R_g), and primary particle diameter (d_p):

$$N_p = k_f\left(\frac{2R_g}{d_p}\right)^{D_f} \tag{7}$$

Fractal dimension (D_f) is the exponent that relates mass to distance from the centre of mass, and is commonly used as a statistical index to describe the complex morphology of soot particles [14,23,50–52]. Chain-like agglomerates are characterised by smaller values of fractal dimension, whilst larger values indicate clusters.

Fractal dimension was calculated in this study via two methods: the Minkowski-Bouligand or so-called 'Box Counting' method [53,54], and an iterative method proposed by Lapuerta et al. [55].

The Minkowski-Bouligand method involves counting the number of boxes (N) with sides of length ε needed to cover the fractal, and observing change in this value as the size of the boxes decrease. The fractal dimension can be found from the slope of a plot of the logarithm of the box size against the logarithm of the box count:

$$D_f = \lim_{\varepsilon \to 0} \frac{\log N(\varepsilon)}{\log\left(1/\varepsilon\right)} \tag{8}$$

The box-counting method gives a maximum fractal dimension of 2, and as such does not approximate the D_f of the 3D particle but gives the fractal dimension of the 2D projection only. This method can also be extended for use with 3D structures, such as brain tomograms [56], where cubes (voxels) are counted as opposed to boxes (pixels). In such cases, measurements are no longer limited to $D_f \leq 2$.

Lapuerta presented an iterative method for calculation of fractal dimension from 2D TEM projections, utilising the following equation [55]:

$$k_f\left(\frac{d_g}{d_p}\right)^{D_f} = \left(\frac{A_{eff}}{A_p}\right)^{z'} \tag{9}$$

Equations were developed for calculating the fractal pre-factor (k_f) and overlapping exponent (z') by establishing boundary conditions based on hypothetical arrangements of primary particles leading to extreme values of D_f ($D_f = 1$ and $D_f = 3$). A shape factor, $m = 1.95$, was included to better match the shape of the potential interpolation between extremes to that of experimental findings. There are several assumptions made in this method, including that all primary particles are considered spherical with diameters of 25 nm, and the 2D radius of gyration is equal to that of the 3D value. Primary particle diameter, radius of gyration, and agglomerate area must also be taken from 2D projection as an initial step. Values for k_f and z' are used to refine D_f, which is in turn used to calculate number of primary particles. This is then used to recalculate improved values for k_f and z', and the process is repeated until D_f converges within acceptable bounds ($1 < D_f < 3$). As opposed to box-counting methods, the establishing of extreme conditions means this method does in fact attempt to provide a value for the fractal dimension of the 3D particle, using values measured from the 2D projections. In this work, fractal dimension was calculated by the described methods using MATLAB and ImageJ.

Using these two methods has provided the chance to assess the performance of a purpose built and soot-specific method of fractal dimension calculation (Lapuerta Iterative) with that of a more general, and limited technique (Box-Counting).

4.3. Radius of gyration

Radius of gyration, R_g, is defined as the distance from the centre of mass of an object to the point at which its total mass would have to be located to have a moment of inertia equal to that of the original object. The following equations show the relationship between R_g and the inertia moment of a particle (I_p). The total inertia moment can be broken down into the sum of inertia moments from each element of the particle volume (m_i), or expressed in terms of total particle mass (m_p) and radius of gyration.

$$R_g = \sqrt{\frac{I_p}{m_p}} \tag{10}$$

$$I_p = \sum m_i r_i^2 \tag{11}$$

$$I_p = m_p R_g^2 \tag{12}$$

$$R_g = \sqrt{\frac{\sum m_i r_i^2}{m_p}} \tag{13}$$

If we simplify to the point where each element of the particle volume is an individual pixel in the TEM image [55], the total mass of the particle becomes $n_{px} m_i$, where n_{px} is the total number of pixels contained within the image region of interest. If it is then

assumed that each pixel contains an equal mass, the final equation above thus becomes:

$$R_g = \sqrt{\frac{\sum_{i=1}^{n_{px}} r_i^2}{n_{px}}} \tag{14}$$

where r_i is the distance from each pixel within the ROI to the centre of mass, and n_{px} is the total number of pixels within the ROI. This method assumes even density throughout the pixels, and calculates a purely 2-dimensional result [55]. That is the radius of gyration of a flat shape, and not an estimation of the 3D result as was the case in the calculation of the number of primary particles.

Determination of radius of gyration via this method was achieved through use of an ImageJ macro alongside the BoneJ plugin.

5. 3D reconstruction of particles

Soot samples were dispersed onto graphene oxide (GO) TEM support films obtained commercially from Agar Scientific. GO films provide an extremely low contrast background, which is crucial to obtaining sufficiently clear images due to the similarly low contrast nature of soot particles. Creation of the tilt-series was performed using the SerialEM program for automated acquisition [39], and image stacks were registered using the SIFT method [57].

For flame-generated soot, a single-axis tilt-series was created by capturing images in 1° increments across a ±60° tilt, and comprised 121 images in total. For soot-in-oil, oils samples were prepared for TEM imaging as described earlier, a single-axis tilt-series was again created across a single ±60° tilt range, comprising 121 images in total. Due to inaccuracies in the image acquisition, only the images from −60° to +51° were suitable for use in the reconstruction.

Prior to reconstruction, alignment of the tilt-series to account for shifts and rotation was achieved by tracking gold-nanoparticle fiducial markers throughout the images using cross-correlation. Gold particles were manually selected in the untilted images and their coordinates in each image were used to calculate the transformations between subsequent images. A least-square analysis was used to compute the best fit for the alignment. Mean residual stresses among the markers were fixed to 0.23. The program uses a variable metric minimisation approach to find the best fit and implement the displacements, rotations, tilts and magnification differences in the tilted views.

In this work reconstructions were performed using IMOD (version 4.7.51) with eTomo [58] on a Lenovo PC with a 3.50 GHz Intel Xeon E5-1620v3 processor (8 CPUs) and 32 GB RAM, using a 64-bit version of Windows 7. Production of the tomogram via the WBP algorithm for the particles in question was completed in around 30 s. The alignment procedure prior to reconstruction (including manual marker correction) averaged around 5 min in total.

Due to lack of segmentation prior to reconstruction, peripheral noise and small particles were present in the tomograms produced. The transparent nature of soot particles in TEM images means that such background structures can easily be confused as part of the agglomerate of interest. As such, manual segmentation (as opposed to automated methods) is required, and is not only time consuming but often hard to repeat. To isolate the particle of interest and produce the 3D model, manual segmentation was performed slice by slice in the tomogram. As the tomograms contained several hundred individual slices, linear interpolation was used to reduce the duration of segmentation. Particle ROI was selected every 5th slice and interpolated between using ImageJ. Any significant deviations could be easily corrected afterwards. Segmentation of FG-soot tomogram (203 slices) took around 1 h and 30 min to complete, whilst the less complex nature of the soot-in-oil particle meant segmentation (197 slices) lasted around 50 min.

5.1. Elongation correction

Due to the 'missing wedge' of information in the tilt-series, reconstructions are elongated in the z-direction [16,38]. Such an elongation increases values of surface area and volume compared to the true values and can affect shape-descripting parameters. This raises concern regarding the fidelity of the results measured from the reconstructions, and as such we attempted to correct for the elongation. As the true size of the particle in the z-direction is unknown we needed to consider the elongation of a structure of well-determined morphology. The fiducial markers, gold nanoparticles deposited on the grid, were used for this purpose, as they were known to be spherical in shape with diameters in a narrow range close to 10 nm. A perfect reconstruction would produce particles with very similar diameters in each of the principal axes, so by reconstructing these particles we were able to compare the mean diameter in the x- & y-directions with the diameter in the z-direction to calculate an elongation factor. A total of 10 gold nanoparticles in each of the tomograms were reconstructed and an average elongation factor of 30% was observed for both species of soot. Accordingly, the segmented tomograms were subjected to compression by reducing the number of slices in the z-direction by the appropriate amount.

Following elongation correction, quantitative measurements of the volume and surface area of reconstructed particles were taken using the open source UCSF Chimera software [59]. Fractal dimension and radius of gyration calculations were performed using a combination of the BoneJ plugin and macros ImageJ [60].

6. Results and discussion

6.1. Flame-generated soot

Fig. 2 shows A_{eff}, N_p, A_s, and V as a function of tilt angle for a particular exhaust soot particle. ROI selection for the particle in question is shown at several selected angles from the tilt series in Fig. 3 (tilt axis parallel to the page, running vertically through the particle).

Mean primary particle diameter (d_p) was determined as 20 nm through ROI selection in TEM images using the open architecture image-processing program, ImageJ. Projection area, A_{eff}, was determined via the same means every 4° in the tilt series, in 31 separate images in total. As determined from the mean primary particle diameter (d_p), the average primary particle area (A_p) was used in conjunction with the projection area (A_{eff}) to calculate the number of primary particles (N_p) comprising the particle at each of the 31 tilt-angles considered. These values of N_p were then substituted into Eqs. (5) and (6) to calculate the agglomerate volume (V) and surface area (A_s) respectively.

Volume and surface area are derived directly from the number of primary particles, and as such the three parameters share an identical variation in values across the tilt-series. The number of primary particles is itself based on the value of the projection area, which accordingly has a very similar variation, albeit at a slightly different scale.

The variation in these four A_{eff}-based parameters is both significant and asymmetric, the exact form being uniquely determined by the 3-dimensional shape of the particle.

For the single flame-generated particle studied, results were recorded across a substantial range; the maximum projection area

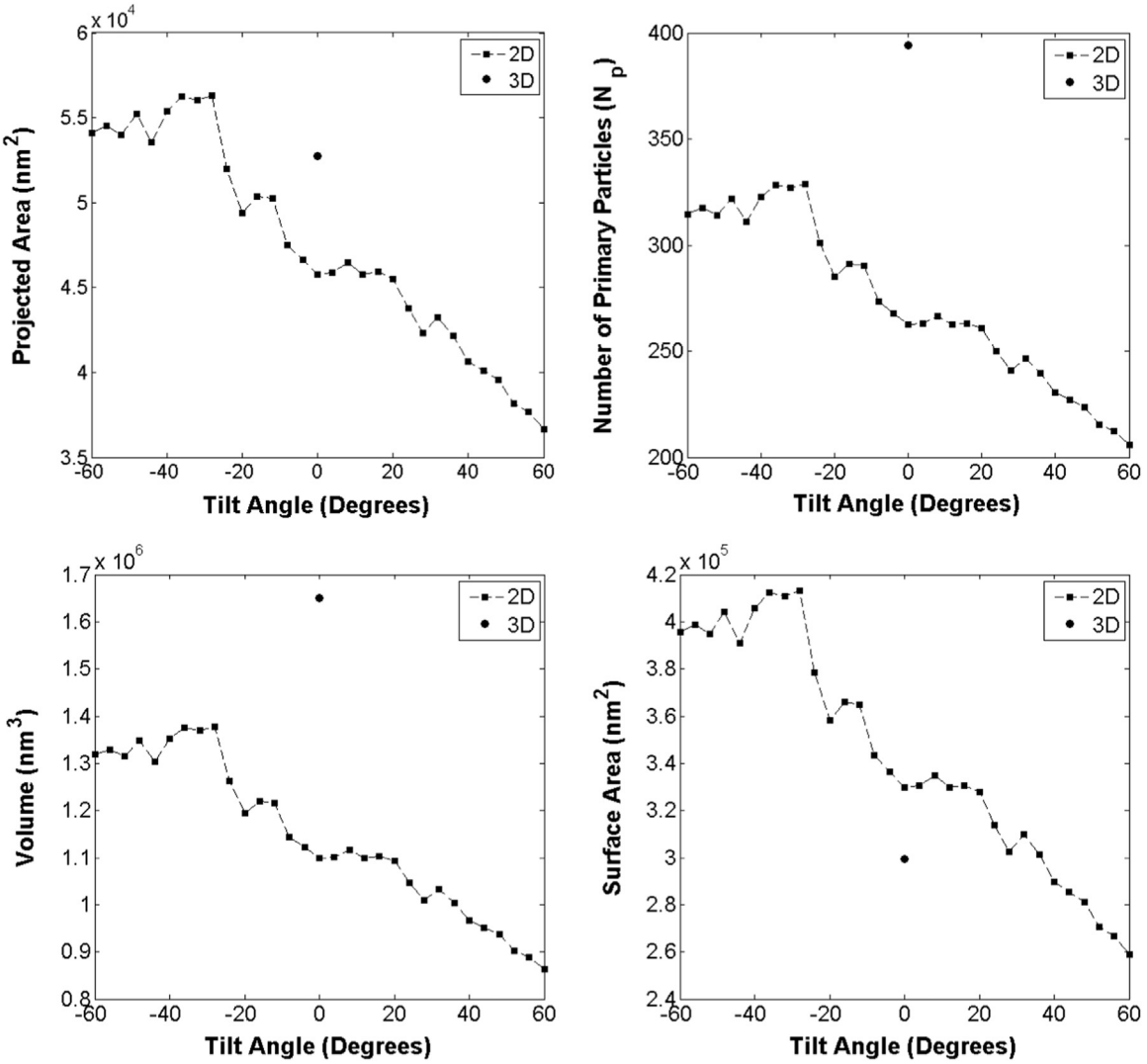

Fig. 2. 2D projection area, number of primary particles, volume, and surface area of flame-generated soot particle as a function of tilt-angle (measured every 4°).

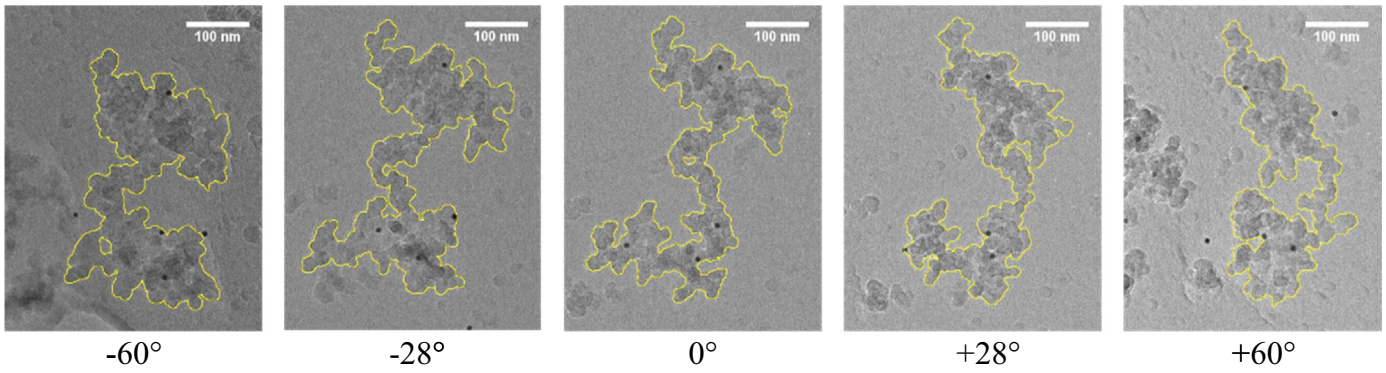

Fig. 3. Projection area of flame-generated soot particle at several angles of tilt.

recorded was 54% larger than the minimum, and the maximum number of primary particles (& therefore maximum volume and surface area) was 60% larger than the minimum recorded.

It was possible to reposition the 3D model of the particle so as to recreate a 2D projection of the particle at 0° tilt. By comparing the A_{eff} of this recalculated projection (denoted as 3D-A_{eff}) with the A_{eff} of the original untilted TEM image, we gain an idea of error in the 3D reconstruction in terms of the x, y-dimensions of the particle. In theory a perfect reconstruction would recreate a 0° projection possessing a projected area equal to that of the original, untilted TEM image. In practice, the 3D-A_{eff} was 15% larger than that of 0° TEM image. The apparent enlargement of the reconstructed particle parallel to the support film may result from blurring and fanning artefacts in the tomogram caused by inaccuracies of the reconstruction method (due to the missing wedge). These artefacts lead to a thickening of the particle that can be exemplified by considering the 0° projection produced from the 3D model (Fig. 4). The area highlighted in pink is considered part

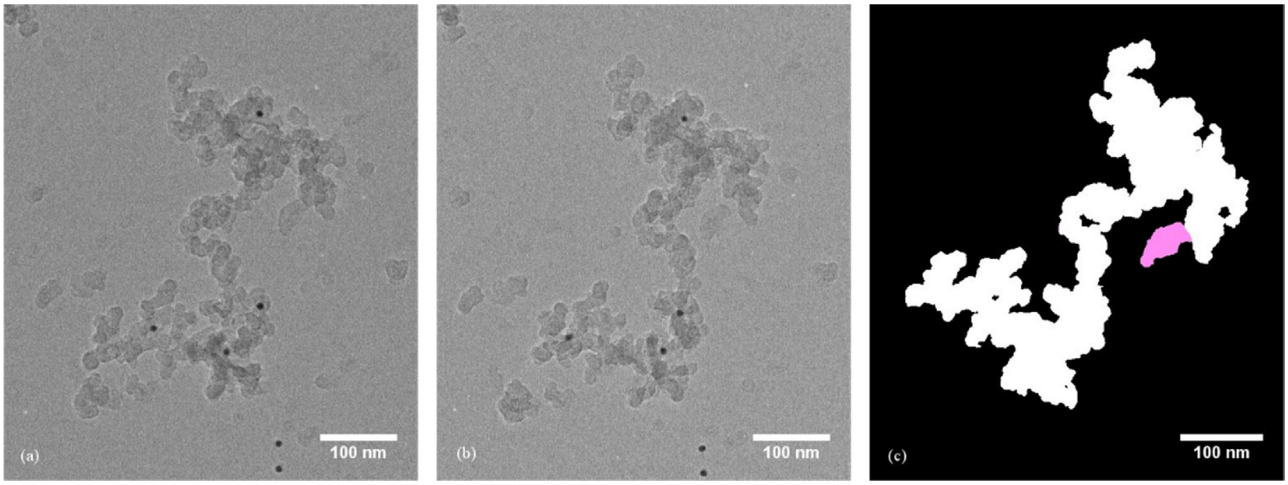

Fig. 4. FG-soot (a) at −13° showing background particle appearing attached, (b) at +6° showing background particle detached and (c) 0° projection from 3D model showing background particle (pink) incorporated into agglomerate. (For interpretation of the references to colour in this figure legend, the reader is referred to the web version of this article).

of the main agglomerate when considering the projected area from tomogram, and whilst appearing attached to the main body in a certain amount of projections is clearly seen to be a separate particle when considering the entire tilt series (Figs. 3 and 4.). If this region is not included in the calculation of 3D-A_{eff}, the difference drops to 11% greater compared to the original projection.

The volume of the reconstructed particle was on average 38% greater than the mean 2D-derived volume, showing a significantly larger underestimation by 2D methods than the 10–20% proposed by Rogak [28]. Number of primary particles is not possible to discern from the 3D model but a theoretically minimum number can be calculated by dividing by the volume of a single primary particle (V_p). As both the 2D- & 3D-derived values of N_p are simply related to the total volume by a factor of $1/V_p$, the difference between 3D and 2D values is the same for N_p as for the total volume (38%).

Contrary to these results, 2D methods on average overestimated the surface area by 13% in comparison to the values derived from the reconstructed particle. This results from the fact that the 2D calculation ignored the loss of internal surface areas within the agglomerate and was as such considered an extreme upper limit.

Fig. 5a shows radius of gyration as a function of tilt angle. Radius of gyration was calculated at each of the 31 images using Eq. (14) with pixel and centre of mass coordinates determined through region of interest selection in ImageJ.

Radius of gyration can be thought of as a measure of complexity, taking into account the distribution of the particle's mass around its centre of mass. Highly branched particles that extend further outward from the centre of mass will exhibit higher R_g values than those that cluster close to the centre, even when their projection area is significantly smaller. As such, the form of the R_g variation is not directly related to that of projection area.

A maximum difference between 2D-derived R_g of 21% is found across the tilt-series, from the maximum close to −30° to the minimum at +60°. Comparison of the variation of R_g with that of A_{eff} highlights the non-direct nature of the relationship between them. A sharp decrease in R_g from −40° to −60° is concurrent with a period of fairly constant projection area, reflecting a relative decrease in the particle's observable complexity.

The underestimation of 2D-derived radii of gyration in comparison to the 3D result was an improvement compared to the

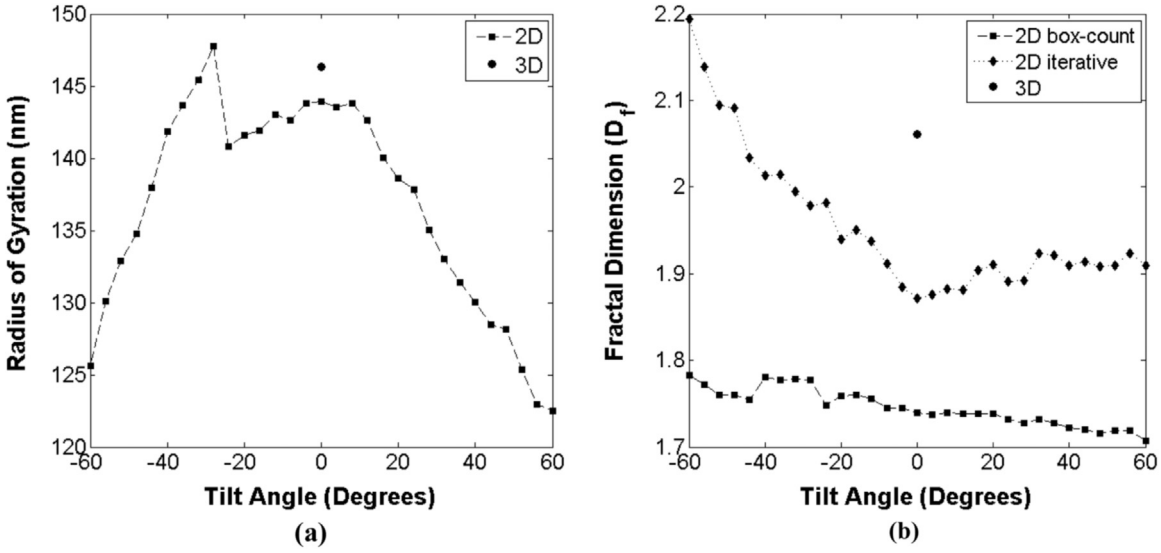

Fig. 5. (a) Radius of gyration of flame-generated soot (every 4°) and (b) fractal dimension of flame-generated soot as calculated by box-counting and iterative methods, including 3D cube counting result, as a function of tilt angle (every 4°).

previously discussed parameters. The pixel-based method showed an average underestimation of just 7%. This result is in contrast to the findings of Köylü et al., where a mean difference of 24% between 3D- and 2D-derived R_g values was observed in their study of simulated aggregates [22]. As mentioned, the pixel-based method is a purely 2D calculation and as such its accuracy in comparison to the 3D result depends on how well the 2D-projections express the 3D character of the particle studied. For example, we would expect a flatter agglomerate (relatively few primary particles thick perpendicular to the TEM film) to be better represented by 2D projections, and thus 2D-R_g results should be more accurate.

Fig. 5b shows the variation of the fractal dimension with tilt angle. Every 4° through the tilt-series, the particle ROI was selected and the box-counting and iterative methods were applied. Box- & cube-counting D_f was calculated using ImageJ and the BoneJ plugin, whilst iterative D_f was calculated by evaluating Eq. (9) using a MATLAB algorithm. Fractal dimension is used to reflect the complexity of particles based on their ability to fill the space around them. Values range from 1 to 3, with a 1 dimensional line possessing $D_f=1$, and a homogeneous 3D sphere having $D_f=3$. As such, particles with their mass clustered close to the centre exhibit high D_f values, whereas highly branched chain-like particles have lower D_f values. This relationship between fractal dimension and branching is opposite to that which was seen for the radius of gyration, our other measure of complexity. Increased branching and chain-like character would, by contrast, cause an increase in the R_g, and as such we expect an inverse relationship between these two parameters to some degree.

Box-counting methods reveal only a modest change in the fractal dimension with tilt angle; with results in the range 1.71–1.79 over the tilt-series (a maximum difference of 4%), and the form of the variation is seen to mimic that of the projection area. This apparent insensitivity to the angle of projection was in contrast to the findings of Wentzel et al. [61], for which the measurement of soot aerosol fractal dimension was seen to vary by up to 20% in 2D projections depending on the orientation. The 3D fractal dimension was found to be 18% larger than the mean 2D box-counting D_f, a result in line with Rogak's findings [28].

Iterative methods show significantly more variation over the tilt-series, with a maximum difference between 2D-derived values of 17%, similar to in Wentzel's study [61]. Despite the relatively greater sensitivity to angle of projection iterative methods proved a much more accurate method of calculating fractal dimension, being on average only a 5% underestimation of the 3D-derived D_f. Iterative results show a roughly parabolic variation over the tilt-series that is, as anticipated, an at least vague inverse of that seen for radius of gyration.

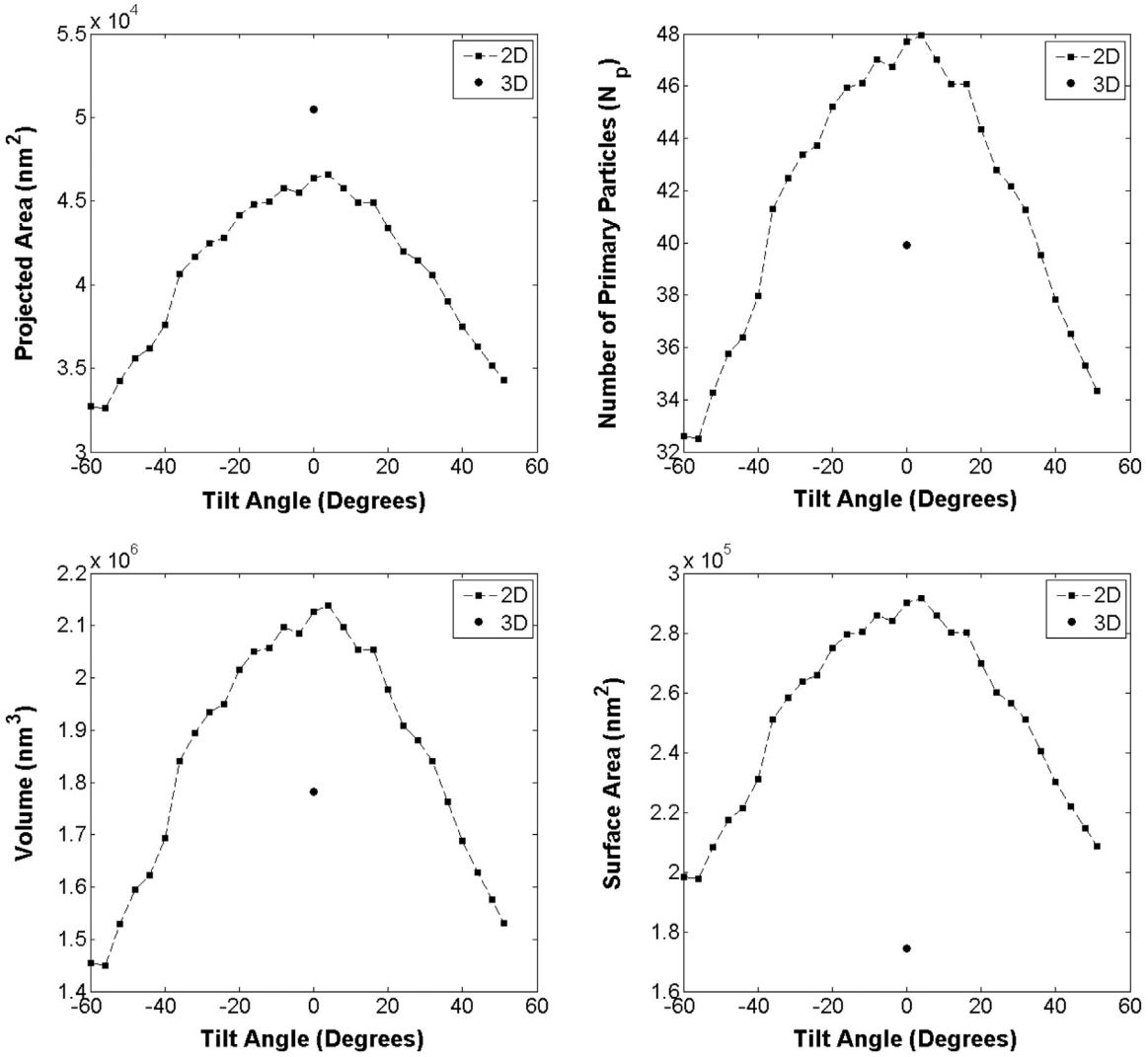

Fig. 6. 2D projection area, number of primary particles, volume, and surface area of soot-in-oil particle as a function of tilt-angle (measured every 4°).

6.2. Soot-in-oil

Fig. 6 shows variation in A_{eff}, N, A_s, and V as a function of tilt angle. Mean primary particle diameter was calculated as 44 nm from ROI selection with ImageJ. Projection area, A_{eff}, was calculated every 4° by similar means. Eq. (1) was evaluated to yield number of primary particles (N_p) at each increment, and using these values of N_p the volume and surface area were calculated using Eqs. (5) and (6) respectively.

As mentioned, the number of primary particles, volume, and surface area are directly related to one another, and all three are based on the projection area. Hence, the manner in which these three parameters vary with tilt-angle is identical, and is essentially identical to that seen for the projection area.

In contrast to the asymmetry observed for the flame-generated soot particle, we now see a strongly parabolic variation centred close to 0°. The parabolic variation derives from the particle being relatively flat, i.e. significantly larger in the x & y dimensions than z, and lying flat on the grid as can be seen in Fig. 1. Inspection of the tilt-series showed the particle to be just a single primary particle thick in the z-direction. The maximum projection area recorded is 43% larger than the minimum, which was located close to the most extreme angles. For N_p, V, and A_s we see a maximum difference of 48% between the largest and smallest values recorded. Again, the shape of the variation of the tilt-series in these four parameters is unique to the particle, arising from its 3-dimensional morphology.

As for the flame-generated particle the reconstructed soot-in-oil model was repositioned to represent the 0° projection, and the area was measured. The 3D-A_{eff} was 9% larger than the area measured from the TEM image, similar to the difference seen for the flame-generated particle when the 'extra' portion was not included in the calculation.

In contrast to the result seen for the FG soot, soot-in-oil found close agreement between 2D- & 3D-derived values of volume and number of primary particles. Prior to the application of the elongation correction to the 3D model, the 2D-methods stood as a 21% underestimate of the 3D value, but the elongation correction reduced this difference to within 4%.

Due to the large overestimation inherent to the calculation of the surface area from projections, the 3D surface area was on average 31% less than the 2D-derived surface areas.

Fig. 7a shows radius of gyration calculated every 4° by substituting pixel and centre of mass coordinates into Eq. (14).

As for the FG soot particle we see this is not directly related to the variation seen in projection area. A large decrease in A_{eff} in the negative direction is accompanied by a fairly steady and globally high R_g value, implying increased branching of the particle despite viewing area decreasing. A maximum difference of 7% is observed between 2D R_g values over the tilt series, a significantly narrower range than seen for FG-soot.

Whilst we have already seen 2D-R_g calculations account well for 3D-R_g values, for soot-in-oil the 2D methods performed even better by providing an average result within 1% of the 3D-R_g.

Fig. 7b shows fractal dimension as a function of tilt angle, evaluated by both iterative and box-counting methods via Eqs. (8) and (9) respectively. Again, Box-counting methods reveal only modest change in the 2D fractal dimension with tilt angle with results in the range 1.73–1.80, a maximum difference of only 4%. The form of the variation is very similar to that of the projection area, as seen for FG-soot.

The 2D methods underestimated the fractal dimension of the 3D model by 10% on average implying the 2D methods were relatively more accurate for the soot-in-oil particle than for FG-soot (18% average difference).

As for the flame-generated soot, the iterative method provided results over a larger range, with a maximum difference between 2D D_f values of 18%.

Where the iterative technique had provided the superior results for FG-soot, the opposite was true for soot-in-oil. As well as an average underestimation of 17% with respect to the 3_D-D_f, the variation of the 2D results closely followed that of the projected area and as such no inverse relationship to R_g, however vague, could be inferred. The results from the iterative method were systematically lower than those from box-counting, a surprising result given that the iterative method is supposed to account for 3D structure whilst box-counting is limited to two dimensions.

7. Discussion

Electron tomography was used as a technique to characterise flame generated carbon black and soot nanoparticles extracted from used oil samples drawn from the sump of a light duty diesel engine. Standard 2D-TEM is an established technique typically used to characterise soot nanoparticles inferring the size, surface

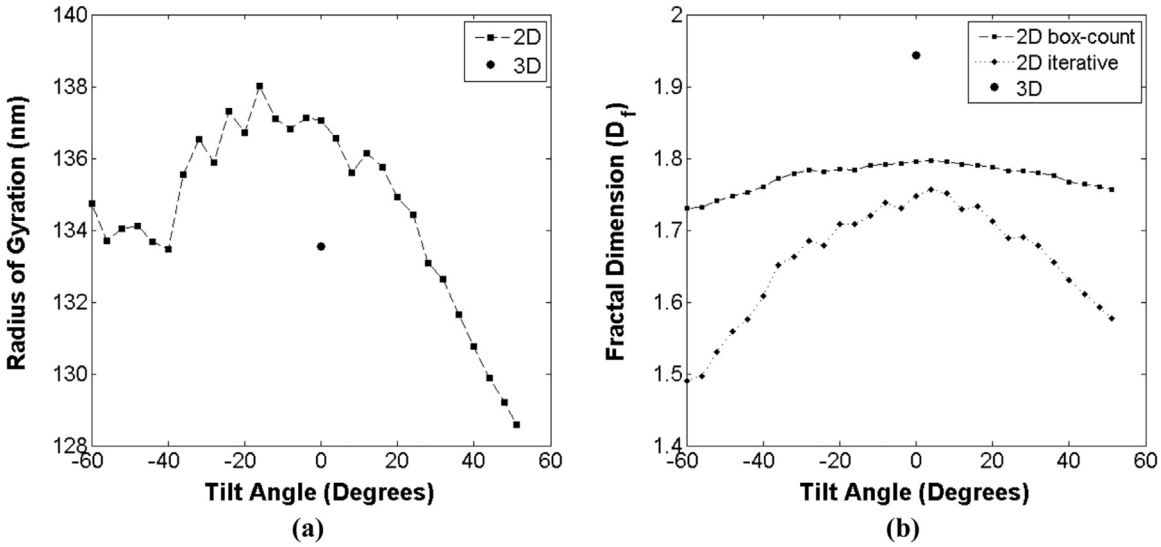

Fig. 7. (a) Radius of gyration of soot-in-oil (every 4°) and (b) fractal dimension of soot-in-oil as calculated by box-counting and iterative methods, including 3D cube counting result, as a function of tilt angle (every 4°).

area and volume measurements from 2D projections, but it has the drawback of underestimating real size and does not provide information on the true shape of the agglomerate. Tomographic reconstruction from the aligned tilt-series images is powerful and well established technique for biological structures or metal nanoparticles. Soot-in-oil analysis is not an area in which 3D-TEM has been applied previously and the experience gained by authors suggests size and morphological parameters information can be generated with relative ease. The understanding of tribological role of soot in oil can be enhanced by measurements of agglomerate surface area and volume.

So-called tilt-series of TEM images were captured every 1° across ±60° tilt-axis for flame-generated soot and soot-in-oil. These tilt-series were used not only for 3D tomographic reconstruction of the particles but also to assess the uncertainties of traditional 2D-derived measurements commonly used when studying carbon nanoparticles. Every 4° throughout a single axis of the tilt-series created, flame-generated soot and soot-in-oil particles were characterised in terms of projection area, volume, surface area, radius of gyration, fractal dimension, and number of primary particles. For comparison, the reconstructed particle volumes were also characterised by the same means.

There was a pronounced difference in primary particle size for the two sources of soot as measured from TEM images, with soot-in-oil being formed from primary particles on average more than twice the size (44 nm) than those that formed the flame-generated soot (20 nm). For both sources of soot, the directly related parameters of A_{eff}, N_p, V, & A_s were seen to be particularly sensitive to the angle of projection in TEM images. Variation in these parameters with tilt-angle was distinct for each of the particles, a reflection of their unique 3D structures. The flame-generated particle showed the greater range to 2D-derived results, with the maximum N_p, V, & A_s values 60% greater than the minimum, compared with a difference of 48% for the soot-in-oil particle. Whilst the sensitivity in these parameters for flame-generated soot is asymmetric across the tilt-series, the relatively 2-dimensional structure of the soot-in-oil particle caused us to observe a strongly parabolic variation about 0° that diminished towards extreme tilt angles.

For flame-generated soot we found that 2D-methods of deriving number of primary particles and volume produced results that were on average a 38% underestimation of the values measured from our 3D model. By contrast, 2D methods on average were in close agreement with the 3D results for the soot-in-oil particle, with a difference of less than 4%. Whilst the flame-generated particle under study had an extensive 3D structure the soot-in-oil particle was notably 2-dimensional, being just a single primary particle thick in the z-direction. Therefore 2D-projections of soot-in-oil were comparatively a better representation of the 3D morphology of the particle, and thus 2D-methods proved superior for this particle.

Due to the inherent overestimation of our 2D-based surface area calculation, for both soots the 2D-3D discrepancy was different than for N_p and V. For flame-generated soot, given that N_p and V were underestimated, this error had the effect of providing a more accurate surface area, being on average 15% greater than the 3D result. For soot-in-oil this overestimation meant that 2D-derived surface area was on average 44% greater than for 3D.

The apparent morphology of the particle in 2D-projections was much more variable for FG-soot and sensitivity of its 2D-derived radius of gyration to the angle of projection was more pronounced, a difference of 21% over the tilt range compared to 7% for soot-in-oil. In comparison with the 3D-derived radius of gyration, the 2D calculation performed well for both particles under study despite the 2D limitations of the method. An average underestimation of only 7% for FG-soot meant the 2D-R_g calculation was a better estimate of the true 3D-value than all but one of the other parameters studied. The average result for soot-in-oil was within 1% of the 3D-derived value, and any associated uncertainty from the spread of 2D results is small due to the relatively insensitive nature of the parameter to angle of projection. As this method calculated a purely 2-dimensional result, that the real 3D-R_g of the flatter, more 2-dimensional soot-in-oil particle was better accounted for by 2D-methods is unsurprising.

The variation in the fractal dimension as calculated by box-counting methods was similar to that of the projection area for both types of soot, and was relatively insensitive to the angle of projection in the tilt series ($<5\%$). Iterative techniques, however, showed more significant variation over the tilt-series, with a maximum difference of close to 18% in both cases. For flame-generated soot, the form of the variation was loosely an inverse to that of radius of gyration, as expected considering the response of each parameter to increased branching of particles. Whilst we observed box-counting methods to underestimate the 3D result to a similar degree to what was seen by Rogak [28], iterative results were superior, being on average within 5% of the 3D-D_f.

Box-counting methods accounted for the 3D-D_f better for soot-in-oil as its flat, 2D structure meant the inherent 2D limitations of the calculation were less pronounced. An unexpected result was that the iterative calculation that had performed so well for flame-generated soot was not only worse than box-counting for soot-in-oil, but gave lower values. The iterative method is supposed to infer 3D-D_f from results measured from 2D projections, allowing us to dissociate from the limitations of the 2D methods that can cause results to be too low [28]. The poor performance of the technique may be due to the peculiarly 2D-nature of the particle, or derive from the fact that the mean primary particle diameter was much larger than that assumed in the derivation of the iterative method (44 nm vs 25 nm) [55].

In this introductory study we have seen that many commonly measured parameters can be highly sensitive to the angle of projection due to significant changes it can cause in the apparent morphology of the particle. Whilst the specific variations in the morphological parameters of flame-generated soot and soot-in-oil were very different, including mean primary particle size, both soot species showed fairly comparable differences over the tilt range. In general, 2D-methods were less sensitive to angle of projection for soot-in-oil, owing to the fact that 2D projections were more representative of the 3D structure of the particle analysed in this work.

We find it acceptable to consider that any 2D projection of a particle is an equally valid representation of the 3-dimensional structure, given that all are equally limited in terms of lacking depth perception. Whilst it may rightly be considered that some orientations of the particle in the tilt-series would be unlikely to result naturally from deposition of the particle upon a TEM grid, given the complex, fractal nature of soot particles it is likely many different orientations would be indeed be possible. As our results suggest great sensitivity to projection angle for many of the commonly considered parameters, it seems almost arbitrary to simply use the result measured from a single, random oriented projection. Given our findings on the sensitivity of parameters to the angle of projection, it raises the question of whether an additional level of uncertainty should be considered when employing traditional, single-projection characterisation of soot. As well as uncertainty relating to a mean result from an ensemble of single-projection results, within each individual result you could consider there to be an uncertainty relating to the sensitivity to angle of projection.

The complexity of the particle under study also seems to affect the overall accuracy of 2D-methods, as while the relatively 2-dimensional soot-in-oil particle found some close agreements

between 2D & 3D-derived results, this was not so much the case for the more 3-dimensional flame-generated particle.

In comparison to 2D-derived methods of characterisation, electron tomography of soot allows us to circumvent many of the issues relating to angle of projection and the 2D limitations of projections (empirical correction factors, approximations, purely 2D results). Whilst some parameters will always require some level of approximation (for example 3D-R_g assumes constant density in all voxels, and 3D-N_p still assumes a constant primary particle diameter) high quality 3D reconstruction could potentially provide much more accurate characterisation. However, many barriers stand in the way of tomographic reconstruction of soot becoming a legitimate alternative to 2D methods. It remains highly time and labour intensive, with subjectivity and elongation/blurring issues affecting the fidelity of measurements from such methods.

8. Conclusions

3D volume reconstruction of flame-generated and soot-in-oil nanoparticles was successfully achieved through the use of bright-field transmission electron microscopy.

Flame-generated particle under study showed an extensive 3D structure; on the contrary, the soot-in-oil particle was notably 2-dimensional, being just a single primary particle thick in the z-direction. The complexity of the particle under study affects the overall accuracy of 2D-methods, as while the relatively 2-dimensional soot-in-oil particle found some close agreements between 2D- and 3D-derived results.

For flame-generated soot volume calculation from 2D measurements produced results that were on average a 38% underestimation of the values measured from our 3D model.

Soot-in-oil found close agreement between 2D- and 3D-derived values of volume and number of primary particles; 2D-methods stood as a 4% underestimate of the 3D value. 3D surface area was on average 31% less than the 2D-derived surface areas; due to the large overestimation inherent to the calculation from projections.

The 2D iterative method underestimated the fractal dimension of the 3D model by 5% for the flame-generated soot, while box counting approach led to an underestimation of 18%. Box counting method was relatively more accurate for estimating the fractal dimension of the soot-in-oil particle with a 10% difference between 2D- and 3D-derived; the iterative method instead showed an average underestimation of 17% with respect to the 3D-D_f.

Many commonly measured parameters to characterise soot can be highly sensitive to the viewing angle due to significant changes it can cause in the apparent morphology of the particle. Uncertainty in morphological parameters calculated from 2D TEM images is then significant, and this study emphasises the potential superiority of values derived from 3D volumes created ET methods.

Acknowledgements

The authors would like to thank Dr C.D.J. Parmenter for his valuable *insights* and *discussion*. The financial support through the scholarship provided by EPSRC DTG Centre in Complex Systems and Processes [Grant number EP/M506588/1] for one of the authors, E. Haffner-Staton, is also acknowledged.

References

[1] La Rocca A, Bonatesta F, Fay MW, Campanella F. Characterisation of soot in oil from a gasoline direct injection engine using Transmission Electron Microscopy. Tribol Int 2015;86:77–84.
[2] Heywood JB. Pollutant formation and control. In: Duffy A, Morris JM, editors. Internal combustion engine fundamentals. New York: McGraw-Hill Publishing Company; 1988. p. 567–667.
[3] Maricq MM, Podsiadlik DH, Brehob DD, Haghgooie M. Particulate emissions from a direct-injection spark-ignition (DISI) engine, SAE Technical Paper 1999-01-1530; 1999.
[4] Velji A, Yeom K, Wagner U, Spicher U, et al. Investigations of the formation and oxidation of soot inside a direct injection spark ignition engine using advanced laser-techniques, SAE Technical Paper 2010-01-0352; 2010.
[5] Lucchini T, D'Errico G, Onorati A, Bonandrini G, Venturoli L, Di Gioia R. Development and application of a computational fluid dynamics methodology to predict fuel–air mixing and sources of soot formation in gasoline direct injection engines. Int J Engine Res 2014;15(5):581–96.
[6] Clague ADH, Donnet JB, Wang TK, Peng JCM. A comparison of diesel engine soot with carbon black. Carbon 1999;37:1553–65.
[7] Richter H, Howard JB. Formation of polycyclic aromatic hydrocarbons and their growth to soot, a review of chemical reaction pathways. Prog Energy Combust Sci 2000;26:565–608.
[8] Ishiguro T, Takatori Y, Akihama K. Microstructure of diesel soot particles probed by electron microscopy: first observation of inner core and outer shell. Combust Flame 1997;108:1–2.
[9] Omidvarborna H, Kumar A, Kim D-S. Recent studies on soot modeling for diesel combustion. Renew Sustain Energy Rev 2015;48:635–47.
[10] Green DA, Lewis R. The effects of soot-contaminated engine oil on wear and friction: a review. Proc Inst Mech Eng Part D: J Automob Eng 2008;222 (9):1669–89.
[11] La Rocca A, Di Liberto G, Shayler PJ, Parmenter CDJ, Fay MW. Application of nanoparticle tracking analysis platform for the measurement of soot-in-oil agglomerates from automotive engines. Tribol Int 2014;70:142–7.
[12] La Rocca A, Di Liberto G, Shayler PJ, Fay MW. The nanostructure of soot-in-oil particles and agglomerates from an automotive diesel engine. Tribol Int 2013;61:80–7.
[13] Su DS, Jentoft RE, Muller JO, Rothe D, Jacob E, Simpson CD, et al. Microstructure and oxidation behaviour of euro IV diesel engine soot: a comparative study with synthetic model soot substances. Catal Today 2004;90:127–32.
[14] Lapuerta M, Ballesteros R, Martos FJ. The effect of diesel engine conditions on the size and morphology of soot particles. Int J Veh Des 2009;50(1):91–106.
[15] Devlin C, Passut C, Campbell R, Jao T. Biodiesel fuel effect on diesel engine lubrication. SAE Technical Paper 2008-01-2375; 2008.
[16] La Rocca A, Fay MW, Campbell J. Soot-in-oil 3D volume reconstruction through the use of electron tomography: an introductory study. Tribol Lett 2016;61:8.
[17] Choi W, Leu MT. Nitric acid uptake and decomposition on black carbon (soot) surfaces: its implications for the upper troposphere and lower stratosphere. J Phys Chem A 1998;102:7618–30.
[18] Neeft JPA, Nijhus TX, Smakman E, Makkee M, Mulijn JA. Kinetics of the oxidation of diesel soot. Fuel 1997;76:1129–36.
[19] Gautam M, Chitoor K, Durbha M, Summers JC. Effect of diesel soot contaminated oil on engine wear – investigation of novel oil formulations. Tribol Int 1999;32:687–99.
[20] Ryason PR, Chan IY, Gilmore JT. Polishing wear by soot. Wear 1990;137:15–24.
[21] Berbezier I, Martin JM, Kapsa PH. The role of carbon in lubricated mild wear. Tribol Int 1986;19:115–22.
[22] Köylü UO, Faeth GM, Farias TL, Carvalho MG. Fractal and projected structure properties of soot aggregates. Combust Flame 1995;100:621–33.
[23] Neer A, Köylü UO. Effect of operating conditions on the size, morphology, and concentration of submicrometer particulates emitted from a diesel engine. Combust Flame 2006;146:142–54.
[24] Park K, Kittelson DB, McMurry PH. Structural properties of diesel exhaust particle measured by transmission electron microscopy (TEM): relationships to particle mass and mobility. Aerosol Sci Technol 2004;33:881–9.
[25] Köylü UO, McEnally CS, Rosner DE, Pfefferle LD. Simultaneous measurements of soot volume fraction and particle size/microstructure in flames using a thermophoretic sampling technique. Combust Flame 1997;110:494–507.
[26] Blake DF, Kato K. Latitudinal distribution of black carbon soot in the upper troposphere and lower stratosphere. J Geophys Res 1993;100:7195–202.
[27] van Poppel LH, Friedrich H, Spinsby J, Chung SH, Seinfeld JH, Buseck PR. Electron tomography of nanoparticle clusters: implications for atmospheric lifetimes and radiative forcing of soot. Geophys Res Lett 2005.
[28] Rogak SN, Flagan RC. Characterization of the structure of agglomerate particles. Part Part Syst Charact 1992;9:19–27.
[29] Patel Mihir, Aswath Pranesh B. Structure and chemistry of crankcase and cylinder soot and tribofilms on piston rings from a Mack T-12 dynamometer engine test. Tribol Int 2014;77:111–21.
[30] Hu E, Hu X, Liu T, Fang L, Dearn KD, Xu H. The role of soot particles in the tribological behaviour of engine lubrication oils. Wear 2013;304:152–61.
[31] Lahouij I, Dassenoy F, Vacher B, Sinha K, Brass DA, Devine M. Understanding the deformation of soot particles/agglomerates in a dynamic contact: TEM in situ compression and shear experiments. Tribol Lett 2014;53:91–9.
[32] Wang Yuesen, Liang Xingyu, Shu Gequn, Dong Lihui, Sun Xiuxiu, Yu Hanzhengnan, et al. Effects of an anti-wear oil additive on the size distribution, morphology, and nanostructure of diesel exhaust particles. Tribol Int 2015;92:379–86.
[33] Uy Dairene, Ford Monica A, Jayne Douglas T, O'Neill Ann E, Haack Larry P, Hangas Jon, et al. Characterization of gasoline soot and comparison to diesel

soot: morphology, chemistry, and wear. Tribol Int 2014;80:198–209.
[34] Cui Jun, Oberoi Sonia, Briggs Stuart, Goldmints Isabella. A viscosity modifier solution to reconcile fuel economy and durability in diesel engines. Tribol Int 2016;101:43–8.
[35] Giechaskiel B, Alfody B, Drossinos Y. A metric for health effects studies of diesel exhaust particles. J Aerosol Sci 2009;40(8):639–51.
[36] Corcione M. Empirical correlating equations for predicting the effective thermal conductivity and dynamic viscosity of nanofluids. Energy Convers Manag 2011;52(1) 798-793.
[37] Adachi K, Chung SH, Friedrich H, Buseck PR. Fractal parameters of individual soot particles determined using electron tomography: implications for optical properties. J Geophys Res 2007;112.
[38] Fernandez J. Computational methods for materials characterization by electron tomography. Curr Opin Solid State Mater Sci 2013;17:93–106.
[39] Mastronarde DN. Automated electron microscope tomography using robust prediction of specimen movements. J Struct Biol 2005;152:36–51.
[40] Batenburg KJ, Sijbers J. DART: a practical reconstruction algorithm for discrete tomography. IEEE Trans Image Process 2011;20(9):2542–53.
[41] Lucic V, Forster F, Baumeister W. Structural studies by electron tomography: from cells to molecules. Ann Rev Biochem 2005;74 883-865.
[42] Li MH, Yang YQ, Huang B, Luo X, Zhang W, Han M, et al. Development of advanced electron tomography in materials science based on TEM and STEM. Trans Nonferr Met Soc China 2014;24:3031–50.
[43] Fernandez J. Computational methods for electron tomography. Micron 2012;43:1010–30.
[44] Bonatesta F, Chiappetta E, La Rocca A. Part-load particulate matter from a GDI engine and the connection with combustion characteristics. Appl Energy 2014;124:366–76.
[45] Medalia AI, Heckman FA. Morphology of aggregates-II. Size and shape factors of carbon black aggregates from electron microscopy. Carbon 1969;7:577–82.
[46] Medalia AI. VI. Effective volume of aggregates of carbon black from electron microscopy; Application to vehicle absorption and to die swell of filled rubber. J Colloid Interface Sci 1970;32:1.
[47] Medalia AI. Calculation of shape and bulkiness factors; Application to computer-simulated random flocs. J Colloid Interface Sci 1967;24:393–404.
[48] Mandelbrot. Fractal geometry of nature.San Fransico: W. H. Freeman and Company; 1977.
[49] Samson RJ, Mulholland GW, Gentry JW. Structural analysis of soot agglomerates. Langmuir 1987;3:272–81.
[50] Lee KO, Cole R, Sekar R, Choi MY, Kang JS, Bae CS, et al. Morphological investigation of the microstructure, dimensions, and fractal geometry of diesel particulates. Proc Combust Inst 2002;29(1):647–53.
[51] Zhu J, Lee KO, Yozgatligil A, Choi MY. Effects of engine operating conditions on morphology, microstructure, and fractal geometry of light-duty diesel engine particulates. Proc Combust Inst 2005;30(2):2781–9.
[52] Annele K, Virtanen K, Ristimäki JM, Vaaraslahti KM, Keskinen J. Effect of engine load on diesel soot particles. Environ Sci Technol 2004;38(9):2551–6.
[53] Sachdeva K, Attri AK. Morphological characterization of carbonaceous aggregates in soot and free fall aerosol samples. Atmos Environ 2008;42 (5):1025–34.
[54] Wozniak M, Onofri FRA, Barbosa S, Yon J, Mroczka J. Comparison of methods to derive morphological parameters of multi-fractal samples of particle aggregates from TEM images. J Aerosol Sci 2012;47:12–26.
[55] Lapuerta M, Ballesteros R, Martos FJ. A method to determine the fractal dimension of diesel soot agglomerates. J Colloid Interface Sci 2006;303:149–58.
[56] Ruiz de Miras J, Navas J, Villoslada P, Esteban FJ. UJA-3DFD: a program to compute the 3D fractal dimension from MRI data. Comput Methods Programs Biomed 2011;104:452.
[57] Lowe DG. Object recognition from local scale-invariant features. In: Proceedings of the Seventh IEEE International Conference on Computer Vision, 2; 1999, p. 1150–1157.
[58] Kremer JR, Mastronarde DN, McIntosh JR. Computer visualization of three-dimensional image data using IMOD. J Struct Biol 1996;116:71–6.
[59] Yang Z, Lasker D, Schneidman-Duhovny D, Webb B, Huang CC, Pettersen EF, et al. UCSF Chimera, MODELLER, and IMP: an integrated modelling system. J Struct Biol 2012;179(3):269–78.
[60] Doube M, Klosowski MM, Arganda-Carreras I, Cordelières FP, Dougherty RP, Jackson JS, et al. BoneJ: free and extensible bone image analysis in Image. J Bone 2010;47(6):1076–9.
[61] Wentzel M, Gorzawski H, Naumann KH, Saathoff H, Weinbruch S. Transmission electron microscopical and aerosol dynamical characterization of soot aerosols. Aerosol Sci 2003;34:1347–70.